

# Structural and Optical Properties of Polymer Blend Nanocomposites Based on Poly (vinyl acetate-co-vinyl alcohol)/TiO<sub>2</sub> Nanoparticles

A. Ismaila<sup>1</sup>, P. O. Akusu<sup>1</sup> and T. O. Ahmed<sup>2\*</sup>

<sup>1</sup>Department of Physics, Ahmadu Bello University, Zaria, Nigeria

<sup>2</sup>Department of Physics, Federal University Lokoja, Kogi, Nigeria

## Research Article

13

## ABSTRACT

Titanium dioxide and organic polymer blend poly (vinyl acetate-co-vinyl alcohol) based nanocomposite membranes were prepared and their chemical structure, phase relationship and optical properties investigated. The Scanning Electron Microscopy (SEM) coupled with Energy Dispersive X-ray Spectroscopy (EDS) analysis reveals TiO<sub>2</sub> to be almost isomorphous ( $\geq 99\%$  phase purity) with spherical particles having diameters in the range 25-40nm. The composites were characterized by Fourier Transform Infra Red (FTIR), SEM, X-Ray Diffraction (XRD) and Ultraviolet-visible (UV-vis) Spectrophotometry. The FTIR Spectroscopy reveals significant absorptions below 900cm<sup>-1</sup> to represent Titanium bonds with organic groups and Oxygen while other prominent functional groups above 900cm<sup>-1</sup> reflect the additivity of polyvinyl alcohol and polyvinyl acetate. It was found that embedding inorganic nanoparticles of TiO<sub>2</sub> into the polymer blend matrix of poly (vinyl acetate-co-vinyl alcohol) allowed for some crystallinity formation and cross-linking of the polymer composites during annealing. The XRD results show more defined peaks assigned to each phase of the composite as the TiO<sub>2</sub> content increases from 1 to 4% weight ratio, thus indicating that Nanoparticle filler remain in the semi-crystalline polymer matrix as a separate crystalline phase, which is in good agreement with the SEM. Finally, the resonant coupling between (UV-vis) light and the collective electronic transitions of polymer nanocomposites are examined using UV-vis Spectrophotometer. The variation in the percentage absorbance and transmittance over wavelength range 200nm-900nm is also attributed to TiO<sub>2</sub> Nanoparticles (Nps) content (1-4%) in the samples.

**Keywords:** Polymer blend; TiO<sub>2</sub> Nanoparticles; Polymer Nanocomposites; Chemical structure; UV-visible light absorber.

\* Tel.:

E-mail address: [tajahmol@yahoo.co.uk](mailto:tajahmol@yahoo.co.uk); [tajahmol@gmail.com](mailto:tajahmol@gmail.com).

## 1. INTRODUCTION

In the last few years, the prospects for polymer blending have been compared to the alloying of metals because it requires little or no extra capital expenditure compared to the production of new polymers. This leverage has led to extensive use of polymer blends in the polymer industry over the last few years. Also, polymer blending offers the possibility of producing a range of polymeric materials with properties completely different from those of the blend constituents [1]. Blend properties are crucially affected by phase morphology and this in turn depends upon a number of factors including the choice of parent polymers, compatibilizers, blend composition, moisture content and the method of blend preparation [2,3]. Because of the significant interest in interfacial interaction between inorganic and organic phases (such as variety of polymer and their blend derivatives) as well as size-dependent phenomena of nanoscale particles, polymer blend nanocomposites are capable of dramatically improving numerous favorable properties without losing the inherent good properties of the polymer phases such as ductility, optical transparency etc. these advantages are never achieved in the conventional polymer composites. In addition, property enhancements in polymer nanocomposites are achieved at a very low loading (<5 wt %) of inorganic nanoparticles while the conventional polymer composites (polymer containing microparticles/micron-sized particles as fillers) usually require much loading of the order of 25-40 wt % [4].

In contrast to the traditional dyes, inorganic semiconductive nanocrystals have more resistant to chemical attacks and low degradation with higher photobleaching, broader excitation wavelength range, narrower and tunable emission spectra [5,6,7,8]. This influence has attracted an enormous research effort leading to a myriad of potential applications in engineering, medicine, biology, electronics and allied industries. Their optical properties have been the center of attraction due to strong size-dependent quantum confinement effect associated with inorganic semiconductive nanocrystals. For the development of novel nanodevices such as electronics and optical devices, various stabilizers (surfactants, polymers or coupling agents) have been employed to modify the surface functionalities of the nanocrystals [9,10], as these nanocrystals are seldom prepared without aggregation. A great deal of attention has been focused on  $\text{TiO}_2$  in contrast to other semiconducting materials, because of its low cost, non-toxicity, chemical stability, resistance to photocorrosion, high photocatalytic activity and high refractive index [11,12]. In the last decade, most studies are mainly focused on the dispersion of nanocrystalline  $\text{TiO}_2$  powder for photocatalysis compared to  $\text{TiO}_2$  thin films due to its higher photocatalytic activity [13]. It is an established fact that a mixture of anatase  $\text{TiO}_2$  and a small percentage of rutile  $\text{TiO}_2$  give optimal photocatalytic efficiency as the anatase phase has a wider band gap of 3.20 eV [14].

Polymer nanocomposites represent a merger between traditional organic and nanosized inorganic materials, resulting in compositions that are truly hybrid. The key to forming such novel materials is adequate understanding and manipulation of the guest-host chemistry, occurring between the polymer and the nanoparticles, in order to obtain a homogenous dispersion and a good contact between polymer and added particle surfaces [15]. Generally, the resultant nanocomposites display enhanced favorable properties such as conductivity, toughness, optical activity, catalytic activity, chemical selectivity etc [16]. These attributes have led to the growing interest and uses in various fields such as military equipments, safety and protective garments, automotive, aerospace, electronic and optical devices. A lot of research works exploiting these aforementioned properties have been carried out for possible applications including flame retardancy, chemical resistance, UV resistance, electrical conductivity, environmental stability, water repellency, magnetic field resistance, radar absorption etc [17, 18, 19, 20, 21].

81

82 In this paper, we report the development of Poly (vinyl acetate-co-vinyl alcohol)/TiO<sub>2</sub>  
83 nanocomposites achieved via a two-stage synthetic route and the relationship between  
84 structural and optical properties of the resulting hybrid Poly(vinyl acetate-co-vinyl  
85 alcohol)/TiO<sub>2</sub> nanocomposites employing Fourier Transform Infrared (FTIR) spectroscopy,  
86 Scanning Electron Microscopy (SEM), X-Ray Diffraction (XRD) analysis and UV-visible  
87 Spectrophotometry.

88

89

90

## 91 2. MATERIAL AND METHODS

92

93 Poly (vinyl acetate-co-vinyl alcohol)/TiO<sub>2</sub> nanocomposites were produced via a two-stage  
94 reaction involving the synthesis of TiO<sub>2</sub> Nanoparticles (Nps) from titanium (IV) chloride  
95 {TiCl<sub>4</sub>, BDH Limited Poole, England} employing hydrothermal technique and subsequent  
96 mixing of modified TiO<sub>2</sub> Nps with Poly(vinyl acetate-co-vinyl alcohol) dissolved in toluene via  
97 one-pot reaction. Surface morphology of the synthesized TiO<sub>2</sub> nanoparticles was observed  
98 using EVOI MA10 (ZEISS) multipurpose scanning electron microscope operating at 20kV  
99 employing secondary electron signals. Four samples of Poly (vinyl acetate-co-vinyl  
100 alcohol)/TiO<sub>2</sub> nanocomposites containing 1-4% of TiO<sub>2</sub> Nps were produced by solution  
101 casting into Petri dishes. The samples were oven dried at temperature lower than the  
102 melting point of the polymer blend for 12hrs and subsequently flat and uniform thin samples  
103 were obtained. The FTIR spectra of all the component reagents, polymer blend and the  
104 prepared nanocomposite samples were obtained using SHIMADZU FTIR-8400S  
105 Spectrophotometer in transmission mode without KBr. The spectra were recorded in the  
106 frequency range from 400 to 4600 cm<sup>-1</sup>, after 25 scans, with resolution of 2cm<sup>-1</sup>. The  
107 positions and intensities of the IR bands were processed with Spectral Analysis software.

108 Surface morphologies of Poly (vinyl acetate-co-vinyl alcohol)/TiO<sub>2</sub> nanocomposites were  
109 observed using EVOI MA10 (ZEISS) multipurpose scanning electron microscope operating  
110 at 20kV employing secondary electron signals at a magnification of 500X and the particle  
111 size distribution was obtained using imaging software (Image-J). The crystallinity of polymer  
112 blend/TiO<sub>2</sub> nanocomposites was observed using X-Ray Diffractometer (Phillips X'pert Pro X-  
113 Ray Diffractometre) employing a 1.54060Å copper X-ray source. The samples were scanned  
114 from 2θ = 5°-80° using a step size of 0.06°. The percentage crystallinity (X<sub>c</sub>) was calculated  
115 following the procedure proposed by [22], with the Scientific Graphing and Data Analysis

116 Software (Origin 8.0), using the following equation:  $X_c = \frac{A_c}{A_c + A_a}$  where X<sub>c</sub>, (percentage

117 crystallinity), is the ratio of crystalline peak area (A<sub>c</sub>) to the sum of the crystalline peak area  
118 (A<sub>c</sub>) and amorphous peak area (A<sub>a</sub>). Finally, the absorption/filtering property of the polymer  
119 blend /TiO<sub>2</sub> nanocomposites was studied in the ultraviolet (UV) radiation wavelength range  
120 of 200nm-400nm and visible radiation wavelength range of 400nm-900nm using JENWAY  
121 6405 UV-visible Spectrophotometer.

122

123

## 124 3. RESULTS AND DISCUSSION

125

126 The image presented in figure 1 together with the corresponding EDS spectra obtained  
127 using characteristic x-rays emitted by TiO<sub>2</sub> nanoparticles was observed at a magnification of  
128 83.04kX. The uniform contrast in the image revealed TiO<sub>2</sub> to be almost isomorphic.

Nevertheless, Oxygen and Nitrogen occur with minor concentrations as impurities thereby making Ti the dominant element with concentration of about 99.5% as depicted in the EDS spectra (fig 1b). The morphology of  $\text{TiO}_2$  nanoparticles is such that the particles are closely packed and spherical in shape. The average diameter of the particles is in the range of 25-40nm reflecting that  $\text{TiO}_2$  nanoparticles are transparent and suitable filler for polymer composite applications.

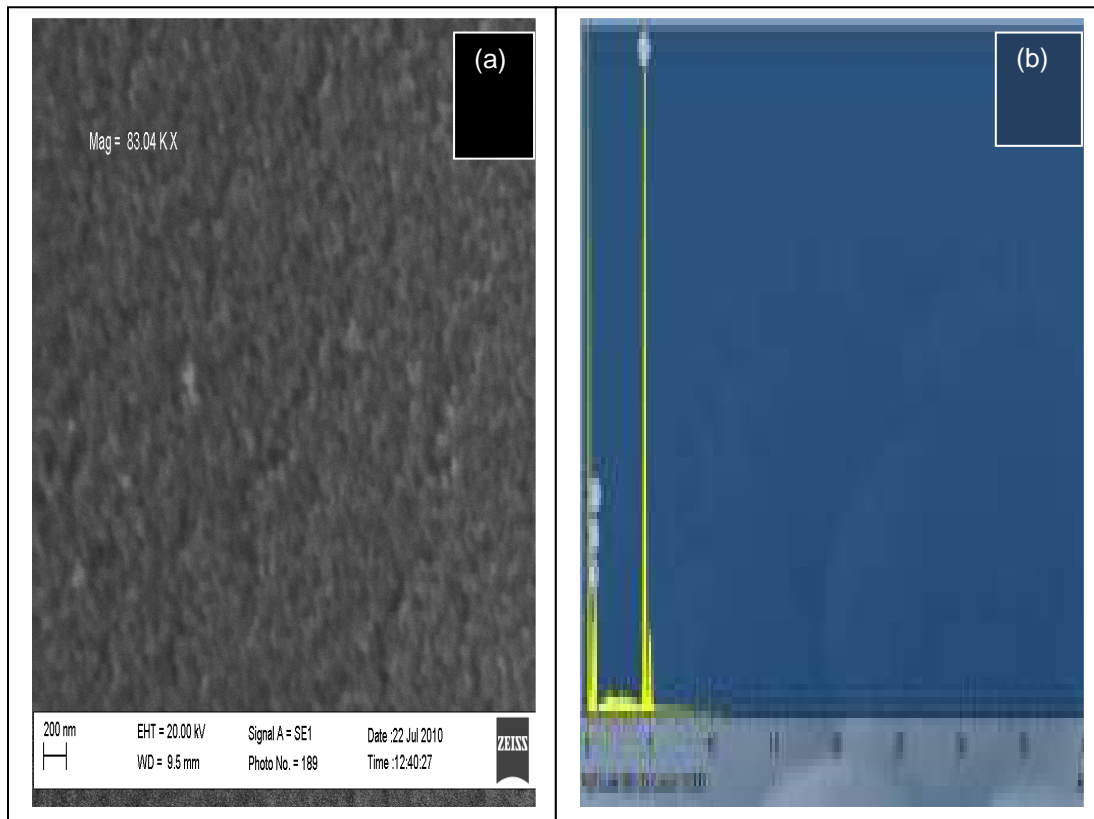


Figure 1: Microstructure and elemental composition of  $\text{TiO}_2$  Nps: (a) SEM image of  $\text{TiO}_2$  Nps (b) EDS spectra of  $\text{TiO}_2$  Nps.

The spectra for the functionalized  $\text{TiO}_2$  nanoparticles, poly (vinyl alcohol), poly (vinyl acetate), polymer blend [poly (vinyl acetate-co-vinyl alcohol)] and the functionalized  $\text{TiO}_2$  are given in figure 2 (a-d) below. It is an established fact that the fundamental vibrations of solids (finger prints) are localized in the low frequency region ( $<1200\text{cm}^{-1}$ ) of the midrange ( $400\text{-}4000\text{cm}^{-1}$ ) of the infrared (IR) spectrum. Also, as reported by [23], the Ti-O bond is clearly located in the range from  $400\text{-}900\text{cm}^{-1}$ . In this work, the significant absorptions observed below  $900\text{cm}^{-1}$  represent Ti bonds with vinyl groups, secondary alcohols, carbonyl groups and oxygen. The prominent functional groups in poly (vinyl alcohol), poly (vinyl acetate) and their blend are OH stretching vibrations,  $\text{CH}_2$  stretching and bending vibrations,  $\text{CH}_3$  bending vibrations, C-O-C vibration in esters,  $\text{vC=O}$  stretching vibration, C-OH stretching vibrations, CH bending and C=O stretching vibration.

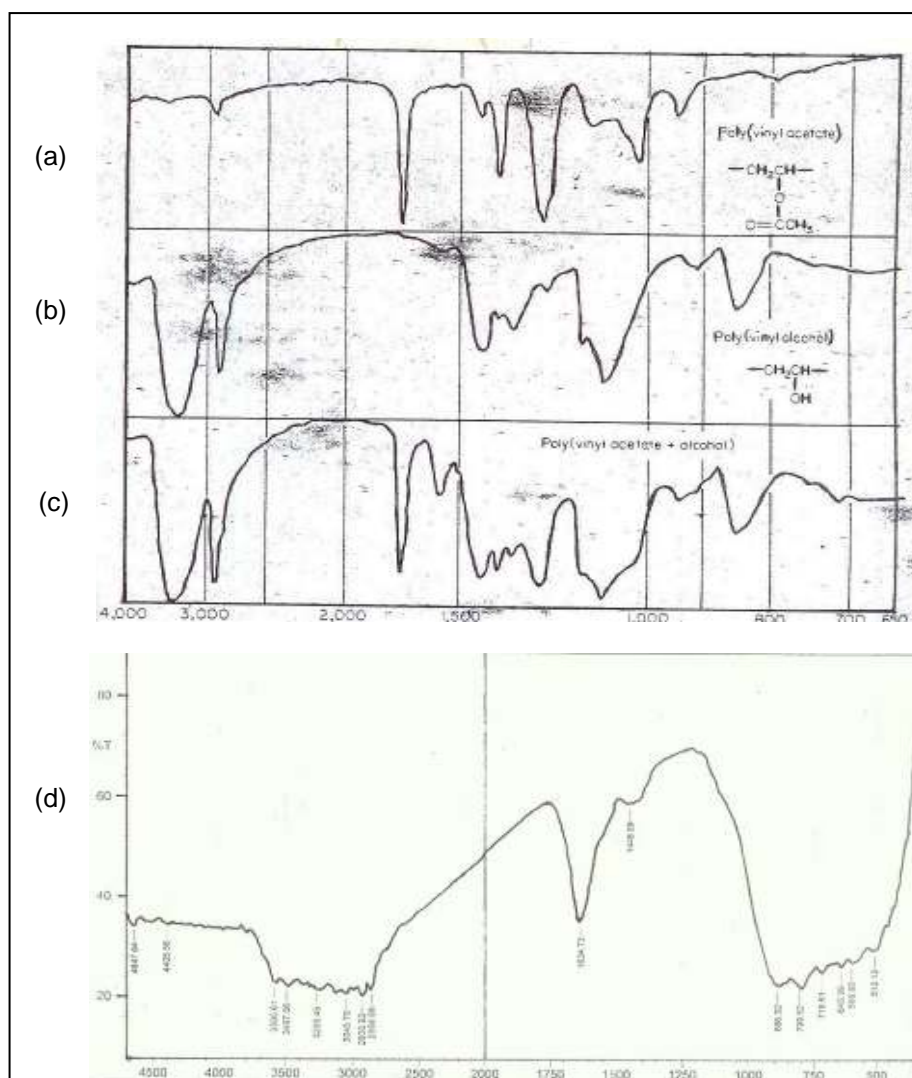


Figure 2: FTIR Spectra of (a) Poly (vinyl alcohol), (b) Poly (vinyl acetate), (c) Polymer blend [poly (vinyl acetate-co-vinyl alcohol)] and (d) functionalized TiO<sub>2</sub> Nps.

From figure 3(a-d), it can equally be deduced that the OH stretching vibrations of the intermolecular hydrogen bonding occurring in the range  $3427.62\text{cm}^{-1}$ - $3483.56\text{cm}^{-1}$  is basically due to the adsorbed H-O-H. Organics (methylene groups) are also represented by the  $\nu_{\text{as}}\text{-CH}_2$  asymmetrical stretching vibrations in ranges slightly above  $2910\text{cm}^{-1}$ . The CH stretching vibrations with coexisting terminal triple bonds resulting from remnant alkynes occur in the range  $2067.76\text{cm}^{-1}$ - $2145.88\text{cm}^{-1}$ . All the changes observed in the vibration frequency of  $\nu\text{C=O}$  in the blend indicates that the incorporation of the nanofillers (TiO<sub>2</sub>) has great influence on the vibration frequency of  $\nu\text{C=O}$ . Furthermore, conjugation with CH<sub>3</sub> (phenyl groups) results in an increase in bond length of C=O thereby creating functional sites on the surface of the polymer blend. The C-O-C vibrations in esters occurring in the frequency ranges  $949.01\text{cm}^{-1}$ - $950.94\text{cm}^{-1}$  and  $1284.63\text{cm}^{-1}$ - $1293.31\text{cm}^{-1}$  represent the possible combination of acetate and alcohol groups. Finally, the functional groups appearing

179 in the range  $383.85\text{cm}^{-1}$ - $491.66\text{cm}^{-1}$  represent Ti-O bonds of the functionalized  $\text{TiO}_2$   
 180 nanoparticles. The observed spectra of the polymer-blend/ $\text{TiO}_2$  nanocomposites reveal the  
 181 additivity of the spectra of polyvinyl alcohol and poly vinyl acetate with the modified  $\text{TiO}_2$   
 182 Nps. In figures 3(a) and 3(b), most of the functional groups peculiar to the component  
 183 reagents were observed but in figures 3(c) and 3(d), chemical reactions between the  
 184 component reagents and the increase in the concentration of the functionalized  $\text{TiO}_2$   
 185 nanoparticles from 2%-4% are responsible for the extinction of the functional groups as a  
 186 result of oxidation and hydrolysis.

187

188

189

190

191

192

193

194

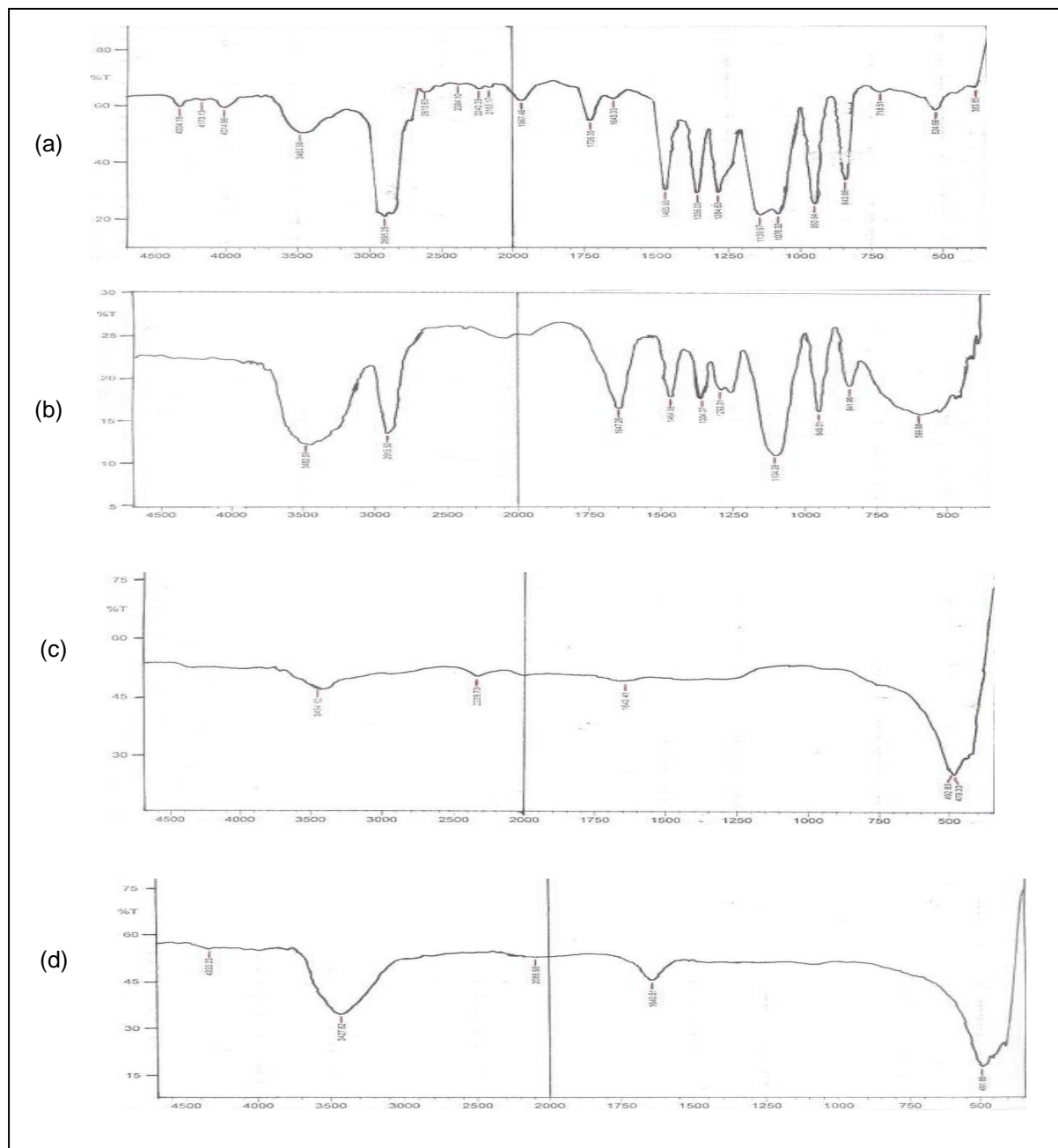
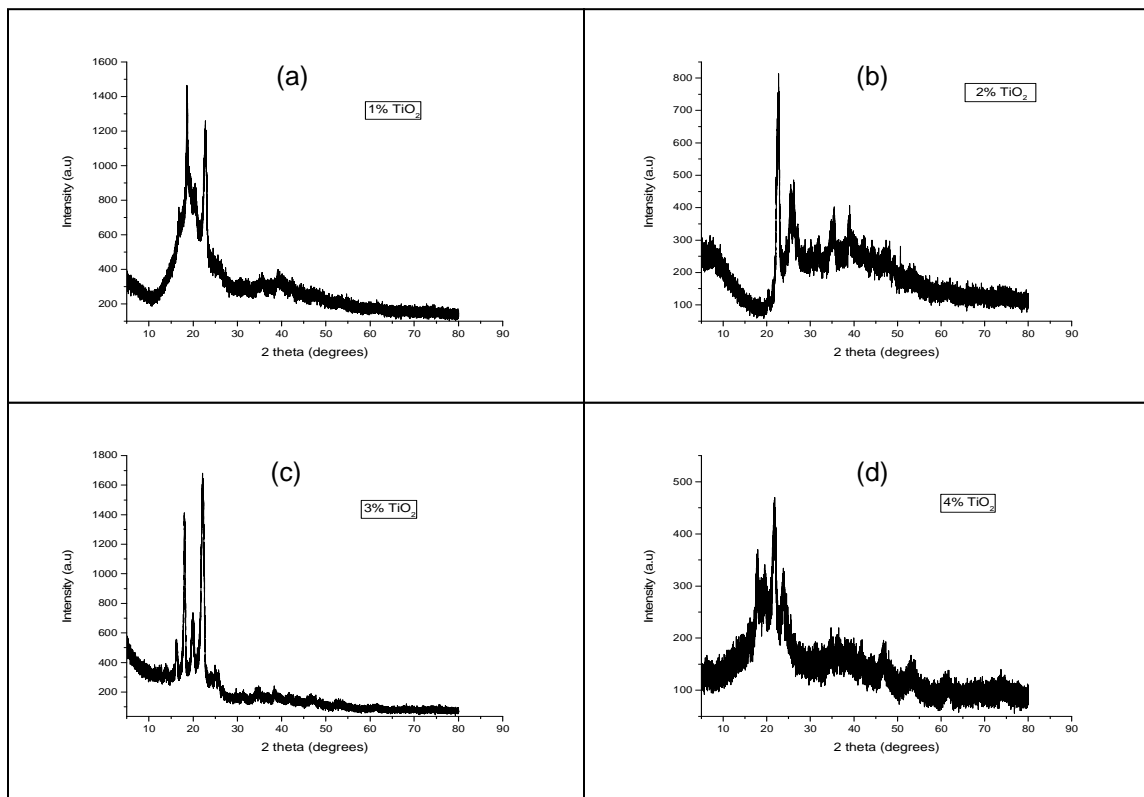


Figure 3: FTIR Spectra of Polymer blend/  $\text{TiO}_2$  Nanocomposites containing: (a) 1% of  $\text{TiO}_2$  Nps (b) 2% of  $\text{TiO}_2$  Nps (c) 3% of  $\text{TiO}_2$  Nps and (d) 4% of  $\text{TiO}_2$  Nps.

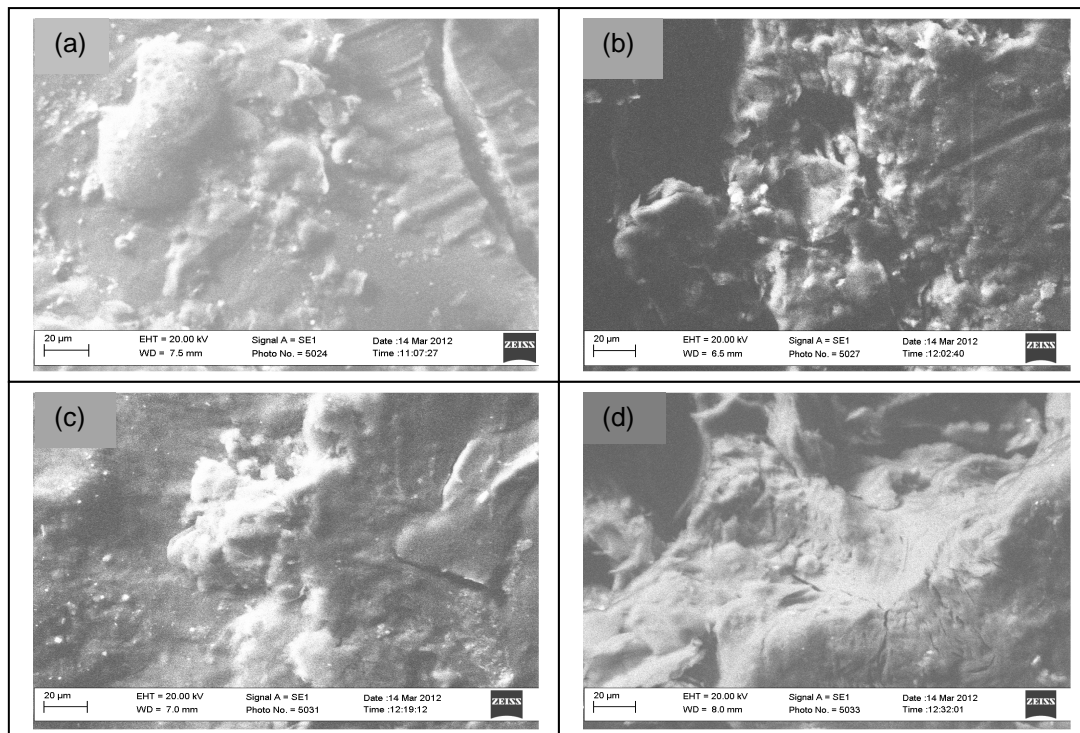


195 The uneven baseline in the XRD patterns seen in figure 4 (a-d) for all the samples is due to  
 196 the large amount of amorphous polymer content. The addition of TiO<sub>2</sub> nanoparticles to the  
 197 polymer blends improved the crystallinity of the composites. The diffraction peaks in the  
 198 range  $2\theta = 15^\circ$ - $20^\circ$  can be linked to crystalline behaviour of the polymer blends. The peaks  
 199 at  $2\theta = 19.66^\circ$ ,  $19.84^\circ$ ,  $20.34^\circ$ , and  $20.49^\circ$  with d-spacings  $d = 4.5154\text{\AA}$ ,  $4.4742\text{\AA}$ ,  $4.3642\text{\AA}$   
 200 and  $4.3325\text{\AA}$  indicate the presence of crystalline structure of PVA, consistent with the works  
 201 of [24, 25]. Furthermore, the XRD patterns of polymer blend/TiO<sub>2</sub> nanocomposites reveal the  
 202 presence of TiO<sub>2</sub> phase but few peaks representing TiO<sub>2</sub> phase have been shifted slightly to  
 203 lower  $2\theta$  values ( $2\theta = 21.91^\circ$ ,  $22.13^\circ$ ,  $22.37^\circ$ ,  $22.45^\circ$ ,  $22.78^\circ$ ,  $22.80^\circ$  and  $22.99^\circ$ ) due to slight  
 204 expansion of TiO<sub>2</sub> crystal structure as a result of surface modification and bonding with the  
 205 polymer blend matrix. This is also consistent with the results presented in some literatures  
 206 [26, 27]. The average crystallite size corresponding to structural order of the pattern  
 207 determined from integral breadth of the peaks according to Scherrer's equation [28] have  
 208 values ranging from  $1688 \pm 290\text{nm}$  to  $4589 \pm 130\text{nm}$ . The percentage crystallinity values of the  
 209 polymer blend/TiO<sub>2</sub> nanocomposites following the procedure proposed by [22] range from  
 210  $56.9 \pm 0.2\%$  to  $67.6 \pm 0.7\%$ . The sample with 4% TiO<sub>2</sub> content displayed higher percentage  
 211 crystallinity compared to other samples.



226 Figure 4: X-ray Diffraction Patterns of Polymer Blend/TiO<sub>2</sub> Nanocomposites containing (a) 1% of  
 227 TiO<sub>2</sub>, (b) 2% of TiO<sub>2</sub>, (c) 3% of TiO<sub>2</sub> and (d) 4% of TiO<sub>2</sub> .  
 228

229 The microstructure of the polymer blend/TiO<sub>2</sub> nanocomposites reveals two distinct phases  
 230 comprising of lighter modified TiO<sub>2</sub> nanoparticles and dark bulk polymer blend matrix. The  
 231 lighter modified TiO<sub>2</sub> nanoparticles are evenly dispersed over the dark bulk polymer matrix  
 232 with spherical shapes and the concentration increased with increasing content of the  
 233 modified TiO<sub>2</sub> NPs (1%-4%) as depicted in figure 5(a-d). The contrast observed in the SEM  
 234 images [figure 5(a-d)] arises from atomic number difference, since phases within a material  
 235 are dependent upon back scattered electron yield and the corresponding atomic number of  
 236 atoms present within different phases. As such, the modified TiO<sub>2</sub> nanoparticles appear  
 237 lighter compared to the bulk polymer blend matrix because the atoms present in TiO<sub>2</sub> phase  
 238 have higher atomic numbers and higher back scattered electron yield. The average particle  
 239 diameters of the polymer-blend/TiO<sub>2</sub> nanocomposites as determined from SEM images  
 240 using imaging software (Image J) range from 119±5µm to 179±4µm.



253 Figure 5: SEM Images of Polymer Blend/TiO<sub>2</sub> Nanocomposites containing: (a) 1% of TiO<sub>2</sub>,  
 254 (b) 2% of TiO<sub>2</sub>, (c) 3% of TiO<sub>2</sub> and (d) 4% of TiO<sub>2</sub>

255 It is a well known fact that changes occur when atoms or impurities are incorporated into a  
 256 pure matrix (polymer, semiconductor, metal etc), because their environment is neither inert  
 257 nor isotropic. Subsequently, exposing the anisotropic matrix (polymer nanocomposites) to  
 258 UV-vis light may lead to resonant coupling between the photons (in this case, UV-vis  
 259 component of the electromagnetic spectrum) and the collective modes (electronic  
 260 transitions/excitations) of the polymer nanocomposites. The interaction of the UV-visible light  
 261 with the polymer nanocomposites possibly will give rise to polarization of the nanocomposite  
 262 matrix, which in turn can be seen as variation in the magnitude of absorption/transmission  
 263 with respect to changes in wavelengths (i.e. 200-900nm) when examined using UV-vis  
 264 spectrophotometer. In addition to this, anisotropy of the nanocomposite matrix resulting from  
 265 addition of TiO<sub>2</sub> nanoparticles gave rise to varied properties as a result of slight structural



modifications. The slight variation in the percentage absorbance over wavelength range (i.e. 200-900nm) is attributed to the TiO<sub>2</sub> nanoparticles content (1-4%) in each sample.

The UV-VIS spectra of polymer blend/TiO<sub>2</sub> nanocomposites are given in figure 6(a-d) below. The plot for polymer blend/TiO<sub>2</sub> sample (containing 1 wt % of nanoparticles) is presented in figure 6(a). The sample filters at the onset of ultraviolet radiation wavelength through 295nm above which it absorbs significantly and rapidly until maximum absorbance of 1.4% is recorded at a wavelength of 390nm. Slightly above the visible range, there is little decline in absorbance but appreciates reasonably through the whole range with maximum recorded at a wavelength of approximately 500nm. The sample displayed excellent property of being an ultraviolet radiation filter at low wavelengths (<300nm) and absorber at higher wavelengths (300-400nm) of the UV range in addition to being an excellent visible absorber. Figure 6(b) portrays the behaviour for polymer blend sample containing 2 wt % of TiO<sub>2</sub> nanofillers. The spectrum shows absolute transparency from the onset of ultraviolet radiation wavelength range through a visible wavelength of 515nm. A much significant absorbance of approximately 3.0%, the maximum, is recorded slightly above that (i.e. at 520nm) from which the absorbance decreases very slightly with a minimum of 2.7% at 800nm. This material is an excellent UV filter and a very good visible radiation absorber.

A similar behaviour to the polymer blend samples described above is observed in both the remaining blend samples (with 3 wt % and 4 wt % of TiO<sub>2</sub> nanofillers respectively) as depicted in figures 6(c) and 6(d). However, there are slight shifts in the onsets of absorption, with the sample containing 3 wt % of TiO<sub>2</sub> having onset at a wavelength of 590nm corresponding to maximum absorbance of approximately 3.0% and that containing 4 wt % of TiO<sub>2</sub> having onset at 550nm corresponding to maximum absorbance of 2.9% as well. The minimum absorbance for these samples are recorded at 795nm (2.8%) and at 780nm (2.7%) respectively. These shifts are attributed to higher content of TiO<sub>2</sub> nanofillers in the polymer blends as TiO<sub>2</sub> are transparent to UV-vis light.

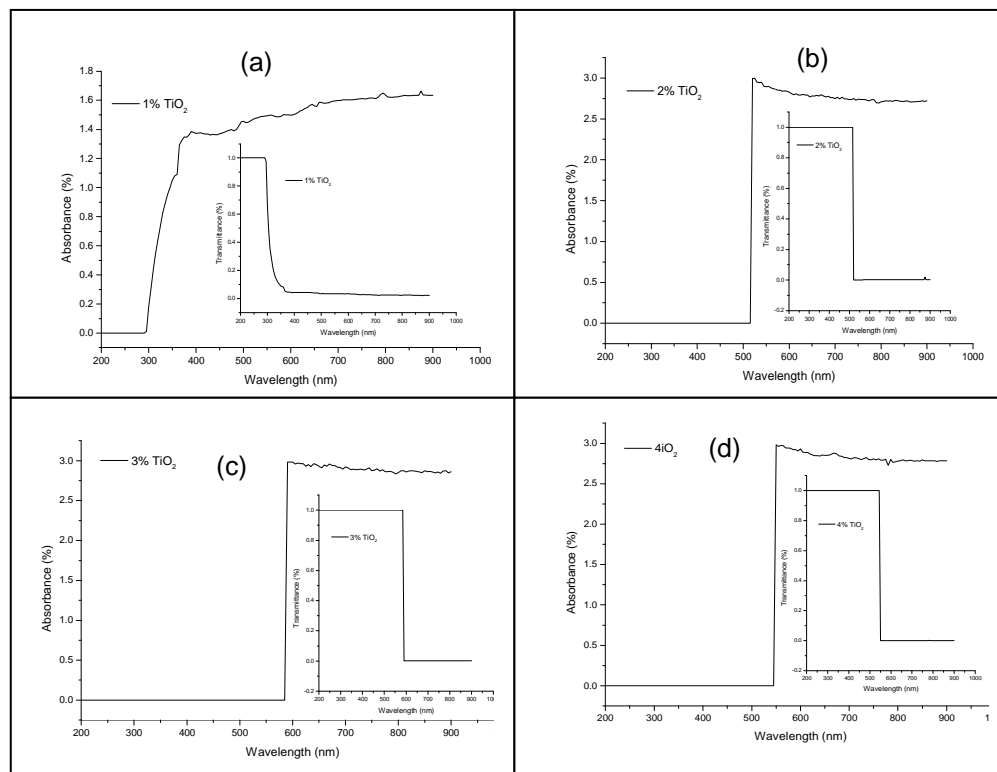


Figure 6: UV-vis spectra of Polymer-Blend/TiO<sub>2</sub> Nanocomposites containing: (a) 1% of TiO<sub>2</sub>, (b) 2% of TiO<sub>2</sub>, (c) 3% of TiO<sub>2</sub> and (d) 4% of TiO<sub>2</sub>.

#### 4. CONCLUSION

The development of the polymer blend nanocomposites was realized by surface modification of TiO<sub>2</sub> Nps in order to create functional sites and improve dispersion of nanoparticles in the polymer blend matrices. FTIR spectroscopy proved the existence of covalent chemical bonding between the polymer chains and inorganic phase in the polymer blend nanocomposites. Thus, revealing significant absorptions below 900cm<sup>-1</sup> to represent titanium bonds with organic groups and oxygen while other prominent functional groups above 900cm<sup>-1</sup> reflect the additivity of polyvinyl acetate and polyvinyl alcohol. X-ray diffraction analysis of the polymer blend nanocomposites revealed an increase in the percentage crystallinity from 56.9 ± 0.2% to 67.6 ± 0.7% for the polymer-blend nanocomposites as TiO<sub>2</sub> nanoparticles content increases from 1% to 4%. Observations from SEM analysis showed that the dispersion of TiO<sub>2</sub> nanoparticles in the polymer matrix was relatively uniform with particles having good adhesion with polymer domains. Investigation with UV-visible spectrophotometer revealed that the dispersion of TiO<sub>2</sub> nanoparticles improved the optical properties of the polymer blends. The fact that nanocomposites displayed some level of transparency at lower wavelengths indicates that the nanoparticles are not agglomerated. In addition, strong UV absorption in some of the nanocomposite samples was observed because of the incorporated TiO<sub>2</sub> particles. In fact, with the exception of sample with 1% content of nanoparticles, all the samples transmit UV radiation and absorb visible radiation at wavelengths of 520nm, 590nm and 550nm respectively. Thus the developed polymer blend nanocomposites could act as an efficient optically transparent UV filter and visible radiation absorber.

#### ACKNOWLEDGEMENTS

We thank Physics Advanced Laboratory, Sheda Science and Technology Complex, Abuja, Nigeria, National Research Institute for Chemical Technology, Zaria, Nigeria and the Multi-users Laboratory, Department of Chemistry, Ahmadu Bello University, Zaria, Nigeria for technical assistance during the experimental characterization.

#### COMPETING INTERESTS

Authors have declared that no competing interests exist.

#### AUTHORS' CONTRIBUTIONS

This work was carried out in collaboration between all authors. Authors TOA and POA designed the study. Author TOA wrote the protocol and wrote the first draft while, author TOA and author IA carried out the experimental work and analyses. Author TOA and author IA managed the literature searches. All authors read and approved the final manuscript.

351

352

## 353 REFERENCES

354

355 1. Wanchoo RK, Sharma PK. Viscometric Study on the Compatibility of some Water  
356 Soluble Polymer-Polymer Mixtures. *Euro. Polym. J.* 2003; 39: 1481-82.

357 2. Dyson RW. *Engineering Polymers*. Chapman and Hall, New York. 1990: 20-28

358 3. Chuu MS, Meyers RR. Effect of Moisture content on the dielectric behaviour of Poly  
359 (vinyl acetate)-Natural Rubber blend. *J Appl Polym Sci.* 1987; 34 (4):1447

360 4. Saujanya C, Radhakrishna S. Polymer Nanocomposites, *J. of Polym. Sci.* 2001:  
361 42: 6723-6731.

362 5. Riegler J, Ditengou F, Palme K, Nann T. Blue Shift of CdSe/ZnS Nanocrystals-  
363 Labels upon DNA-Hybridization. *J. Nanobiotechnol.* 2008; 6(1): 7.

364 6. Bruchez Jr. M, Moronne M, Gin P, Weiss S, Alivisatos AP. Semiconductor  
365 Nanocrystals as Fluorescent Biological labels. *Science.* 1998; 281(5385):2013–  
366 2016.

367 7. Chan WCW, Nie S. Quantum Dot Bioconjugates for Ultrasensitive Nonisotopic  
368 Detection Science. 1998; 281(5385): 2016–2018.

369 8. Jaiswal J, Mattoussi H, Mauro J, Simon S. Long-term multiple Color Imaging of Live  
370 Cells Using Quantum Dot Bioconjugates. *Nat. Biotechnol.* 2003; 21(1): 47–51.

371 9. Patra MK, Manoth M, Singh VK, Gowd GS, Choudhry VS, Vadera SR, Kumar N.  
372 Synthesis of Stable Dispersion of ZnO Quantum Dots in Aqueous Medium Showing  
373 visible Emission from Bluish-Green to Yellow. *J. Lumin.* 2009; 129 (3):320–324.

374 10. Guo Z, Kumar C, Henry LL, Domes EE, Hormes J, Podlaha EJ. Displacement  
375 Synthesis of Cu Shells Surrounding Co Nanoparticles. *J. Electrochem. Soc.* 2005:  
376 152(1): D1–D5.

377 11. Legrini O, Oliveros E, Braun AM, Photochemical Processes for Water Treatment.  
378 *Chem. Rev.* 1993; 93(2): 671-698.

379 12. Sugimoto T, Zhou X, Muramatsu A. Synthesis of Uniform Anatase TiO<sub>2</sub>  
380 Nanoparticles by Gel-Sol Method: 3. Formation Process & Size Control. *J. Colloid*  
381 *Interface Sci.* 2003; 259(1): 43-52.

382 13. Jiaguo Y, Jimmy CYU, Cheng B, Zhao X. Photocatalytic Activity & Characterization  
383 of the Sol-Gel Derived Pb-Doped TiO<sub>2</sub> Thin-films *J. Sol-Gel Sci. Tech.* 2002; 24(1)  
384 39-48.

385 14. Bouras P, Stathatos E, Lianos P. Pure versus Metal-ion-doped Nanocrystalline  
386 Titania for Photocatalysis. *Appl. Catal. B:Environ.* 2007; 73(1-2): 51-59.

387 15. Lagashetty A, Venkataramen I. *Polymer Nanocomposites*. John Wiley and sons.  
388 2005.

- 389 16. Garcia C, Maria M, Dela L. Polymer-Inorganic Nanocomposites: Influence of  
390 Colloidal Silica, A PhD thesis submitted to the university of Twente, Netherlands.  
391 2004.
- 392 17. Mohan S, Lauren NC, Surya SG, Karen IW. Melt Intercalation of Polystyrene in  
393 Layered Silicates, J. of Polym. Sci.: part B: Polym. Physics. 1996: 34: 1433-1449.
- 394 18. Lee SS, Lee CS, Kim MH, Kwak SY, Park M, Lim S, Choe CR, Kim J. Specific  
395 Interaction Governing the Melt Intercalation of Clay with Poly(styrene-co-  
396 acrylonitrile) Copolymers. J. of Polym. Sci.: part B: Polym. Physics. 2001: 39: 2430-  
397 2435.
- 398 19. Pegoretti A, Dorigato A, Penati A. A Tensile Mechanical Response of Polyethylene-  
399 Clay Nanocomposites. Express Polymer Letters. 2007: 1(3): 123-131.
- 400 20. Tolstov AL, Matyushov VF, Klymchok, DO. Synthesis and Characterization of Hybrid  
401 Cured Poly (ether-urethane) Acrylate/Titania Microcomposites Formed from  
402 Tetraalkoxytitanate Precursors, Express Polymer Letters. 2008: 2(6) 449-459.
- 403 21. Manias E, Zhang J, Huh JY. Polyethylene Nanocomposite Heat Sealants with a  
404 Versatile Peelable Character, Macromol. Rapid Commun. 2009: 30: 17-23.
- 405 22. Eichhorn S J, Young RJ. The Young's modulus of Microcrystalline cellulose.  
406 Cellulose. 2001: 8: 197-207.
- 407 23. Morterra C, Magnacca G. A case Study: Surface Chemistry & Structure of Catalytic  
408 Aluminas as Studied by Vibrational Spectroscopy of Adsorbed species" Catal.Today.  
409 1996: 27: (3-4): 497-532.
- 410 24. G'eminarda JC, Bonraya DH. Thermal Conductivity Associated with a Bead-Bead  
411 Content Decorated by a Liquid Bridge; An Experimental Study Based on the  
412 Response of a Chain Subjected to Thermal Cycles. Gayvallet Eur, Phys. 2005:  
413 48: 509-517.
- 414 25. Lee GW, Park M, Kim J, Lee JI, Yoon HG. Enhanced thermal conductivity of  
415 polymer Composites filled with hybrid filler. Composites Part A: Applied Science and  
416 Manufacturing. 2006: 37: 727-734.
- 417 26. Shuqiang J, Hongmin Z. Electrolysis of  $Ti_2CO$  Solid Solution Prepared by  $TiC$  &  
418  $TiO_2$ , Journal of Alloys & Compounds. 2007: 2007: 438: 243-246.
- 419 27. Yang Z, Choi D, Kerisit S, Rosso KM, Wang D, Zhang Z, Graffi G, Liu  
420 J. Nanostructures and Lithium Electrochemical Reactivity of Lithium titanates and  
421 Titanium oxides: A Review. Journal of Power Sources. 2009: 192(2): 588-598.
- 422 28. Patterson AL. The Scherrer formula for X-ray particle size determination. Physical  
423 Review. 1939: 56(10): 978-982.

424  
425  
426  
427  
428